ACS APPLIED MATERIALS & INTERFACES

www.acsami.org

Research Article

Refillable Fuel-Loading Microshell Motors for Persistent Motion in a Fuel-Free Environment

Dong Wang,‡ Chengtao Chen,‡ Jun Sun, Hang Ao, Wencheng Xiao, Huangxian Ju,* and Jie Wu*

Cite This: *ACS Appl. Mater. Interfaces* 2022, 14, 27074−27082

Read Online

ACCESS | Metrics & More | Article Recommendations | Supporting Information

ABSTRACT: Artificial micro-/nanomotors that harvest environmental energy to move require energy surroundings; thus, their motion generally occurs in fuel solutions or under the real-time stimuli of external energy sources. Herein, inspired by vehicles, a refillable fuel-loading micromotor is proposed based on a 2 μm hemispherical multimetallic shell using catalase or platinum on its concave surface as the engine and the bowl structure as the fuel tank. H_2O_2 fuel is drawn into the microbowl by capillary action and restricted inside the bowl space through a self-generated O_2 bubble cap on the microshell mouth. The periodic growth and burst of the O_2 cap cause the enhanced diffusion motion of micromotors. This motion behavior can last for at least 30 min in a fuel-free environment with one H_2O_2 fueling. Additionally, the micromotor can be refilled repeatedly to achieve permanent motion. This demonstration of a refillable fuel-loading micromotor provides a model design of an energy built-in micromotor.

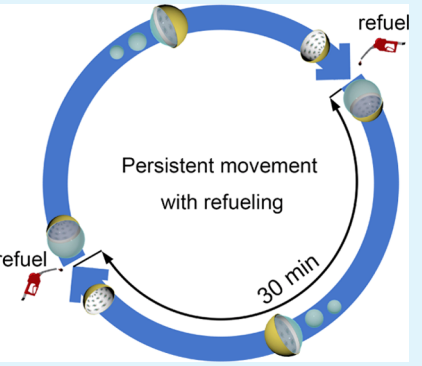

KEYWORDS: *micromotor, microshell, fuel loading, refueling, bubble propulsion*

1. INTRODUCTION

Micro-/nanomotors, owing to their automatic motion, have become popular in many fields, such as biosensing,[1] drug delivery,[2] microtherapy,[3] and environmental remediation.[4] Similar to biological motors, artificial micro-/nanomotors also harvest environmental energy to move and accomplish on-demand tasks. The driving force of micro-/nanomotors comes from the energy conversion of chemical/biochemical reactions,[5,6] acoustic waves,[7] light,[8] magnetic,[9] electric fields,[10] or their combined field.[11] To date, various micro-/nanomotors of different shapes have been prepared from different materials.[12−15] Unfortunately, most micro-/nanomotors need to be present in energy supply surroundings, for example, existence in fuel solutions of H_2O_2,[16] N_2H_4,[17] and Ag^+,[18] or with real-time stimuli of external energy sources,[19−21] which greatly limit their applications, especially in the biological field.

An attractive way to address the demand for external energy sources is the development of micro-/nanomotors using biological fluids as fuel. For example, researchers have used the glucose oxidase (GOx)-catalase bienzymatic reaction to replace the Pt/H_2O_2 reaction and prepare glucose-driven micromotors.[22,23] Additionally, by equipping the urease engine, urea-driven micromotors have been provided with an ionic diffusion phoresis mechanism.[24,25] Moreover, water-fueled micromotors have been fabricated based on the H_2 bubble production of active metals (Mg, Zn, and Al).[26−28] Although these micro-/nanomotors have realized motion with biofuels, they are still limited by challenges of the fuel concentrations above their physiological concentrations, a short lifetime, and acidic reaction conditions.

Chemotactic micro-/nanomotor whose motion mechanism imitates the chemotactic migration in living systems is another type of motor that can perform automatic motion without the requirement of an external energy supply. These motors are generally prepared by putting specific biomolecular coats, including DNase and cell membranes on the surface of micro-/nanomaterials.[29,30] Chemotactic micro-/nanomotors can be activated by physiological targets and conduct automatic tracking movement. However, their exploration is still in the preliminary stage; even more, they face the difficulty of motion in a wide range of ambiences owing to their high specificity.

As we all know, vehicles in a macroscopic world can run freely on different types of roads because of the built-in fuel tank or battery, which can provide energy for movement regardless of the external environment. Thus, we wonder whether we can design micromotors with a built-in fuel tank that can solve the driving energy problem in essence. The catalytic combination of Pt (or catalase)/H_2O_2 is the most widely used engine-fuel pattern in micro-/nanomotors in which Pt (or catalase) catalyzes the decomposition of H_2O_2 into water and O_2, making the motors at different sizes to perform enhanced diffusion, phoresis, or bubble propulsion

Received: March 28, 2022
Accepted: May 24, 2022
Published: June 6, 2022

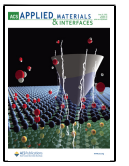

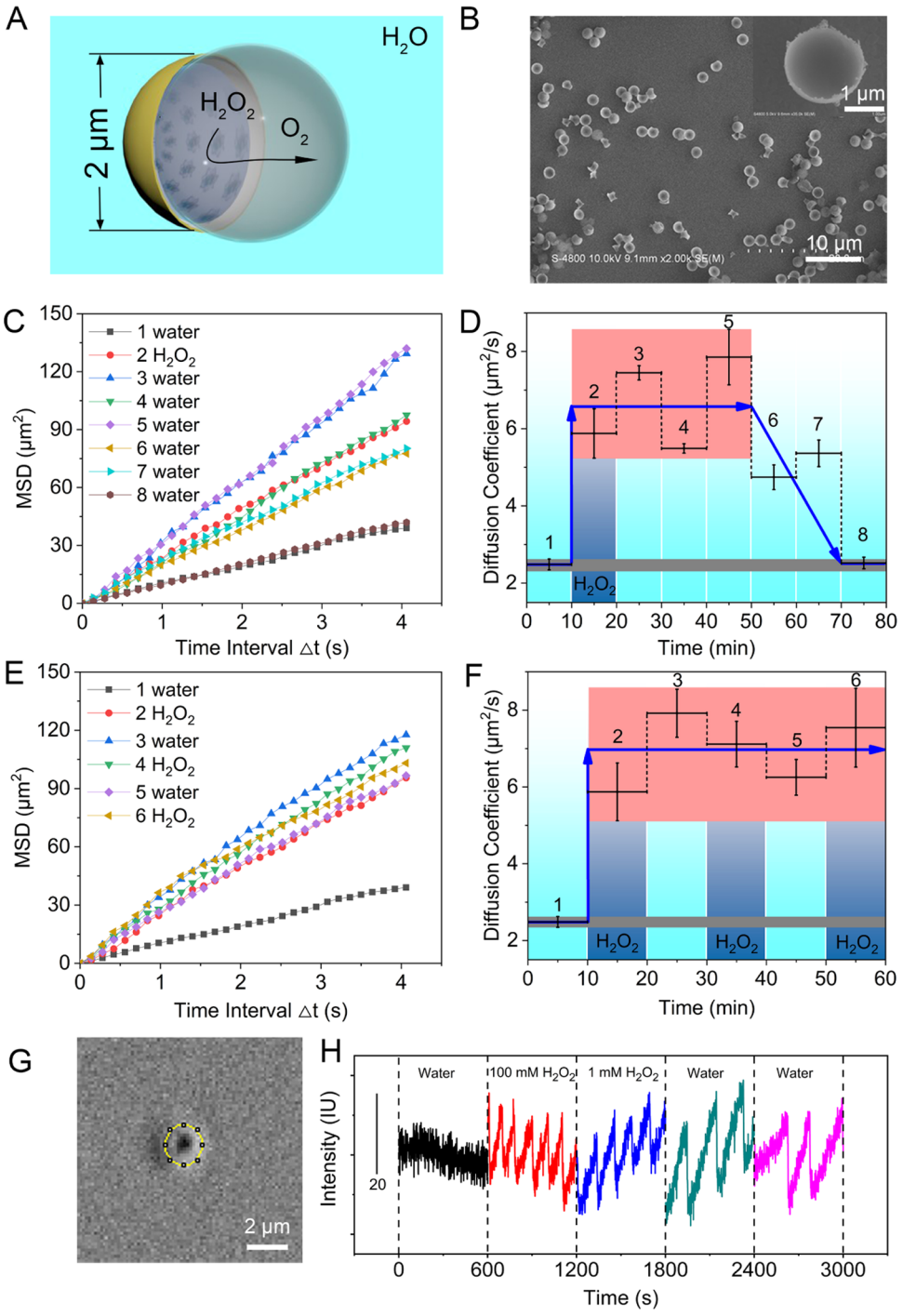

Figure 1. (A) Schematic generation of O_2 bubble on FLM-C. (B) SEM images of FLM-C. (C, E) Average MSD plots and (D, F) the corresponding diffusion coefficients of FLM-C successively in (C, D) and alternately in (E, F) water and 500 mM H_2O_2 solution. (G) Microscope image of immobilized FLM-C with opening upward. (H) Continuous intensity curves of FLM-C soaked successively in different solvents.

motions.[31−33] Herein, based on this popular Pt (or catalase)/H_2O_2 combination, we constructed a refillable fuel-loading micromotor (FLM) using a 2 μm hemispherical shell structure (Figure 1A). Catalase or Pt covered on the concave surface of the microshell was used as the motor engine, and the concave bowl space of the microshell served as the fuel tank to load H_2O_2 fuel. H_2O_2 refueling was achieved through capillary action, and the fuel seal in the microbowl was obtained by a self-produced spherical-cap-shaped O_2 bubble covering the microshell mouth. This FLM was verified to perform continuous motion for more than 30 min with one fueling, along with the property of repeated refueling. The proposed FLM avoided the requirement of external energy sources and could make movement regardless of the surrounding, which provided an insight into fabricating energy built-in micro-/nanomotors for various applications.

2. RESULTS AND DISCUSSION

2.1. Motion of FLM with a Catalase Engine. The fuel-loading micromotor with a catalase engine (FLM-C) was

https://doi.org/10.1021/acsami.2c05442
ACS Appl. Mater. Interfaces 2022, 14, 27074−27082

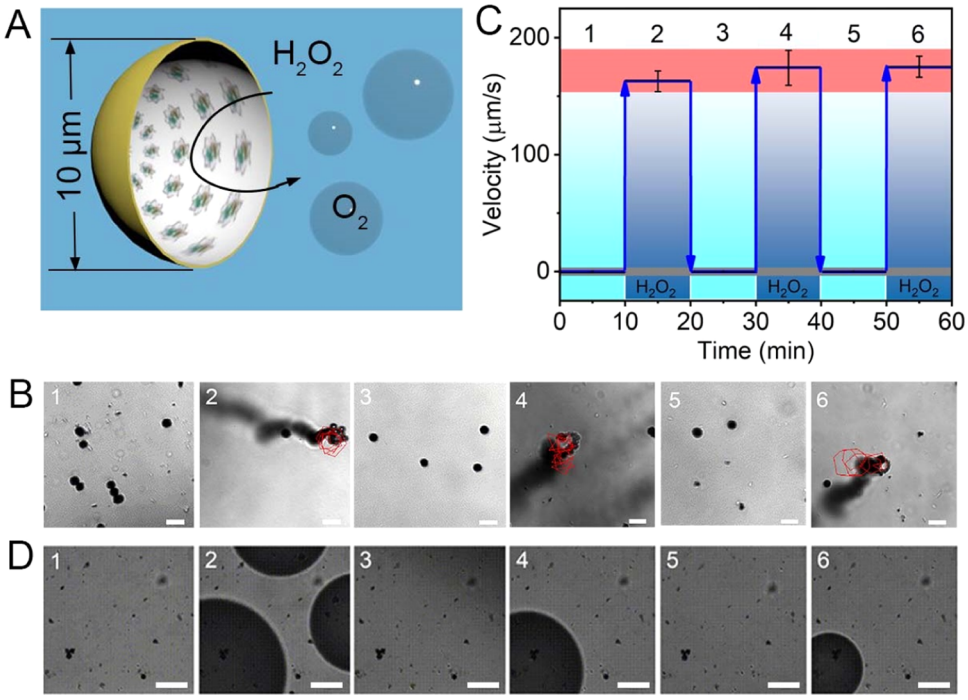

Figure 2. (A) Schematic generation of O_2 bubbles on 10-HSM-C. (B) Motion trajectories, (C) mean velocities, and (D) O_2 bubble generation of 10-HSM-C alternately in water (1,3,5) and H_2O_2 fuel (2,4,6). Scale bars were 10 μm (B) and 50 μm (D).

fabricated by asymmetric modification of catalase on a concave surface of a 2 μm semienclosed Au/Ag/Au multimetallic shell (Figures 1B and S1). The FLM-C exhibited enhanced diffusion when it was presented in H_2O_2 fuel; besides, the persistence of motion behavior was observed after motors were exchanged with the pure water (Video S1). Based on the trajectories of micromotors successively from water to H_2O_2 and then back to water (Figure S2), mean-square-displacement (MSD) curves were extracted, and all showed a linear relationship with the time interval (Δt) (Figure 1C). The diffusion coefficient (D, calculated from MSD = $4D\Delta t$) of FLM-C remained at the high level (~6.7 $\mu m^2/s$) for more than 30 min, including 3 times of water change after one H_2O_2 refueling. Afterward, the enhanced diffusion behavior of FLM-C gradually decreased to a Brownian motion along with the decrease of D (~2.5 $\mu m^2/s$) due to the fuel exhaustion (Figure 1D). These results indicated that the FLM-C was able to load fuel and perform continuous motion in a fuel-free environment.

Additionally, we investigated the refueling ability of FLM-C by alternately placing it in water and H_2O_2 (Video S2). The tracking trajectories (Figure S3) and their corresponding MSD plots (Figure 1E) exhibited that FLM-C could keep vigorous motions with regular H_2O_2 charging, and the D value remained stubbornly high (~6.9 $\mu m^2/s$) in 50 min with two refuelings (Figure 1F). This finding suggested that the FLM-C was refillable and could achieve permanent motion by regular refueling.

The FLM-C that exhibited persistent motion in a fuel-free environment was supposed to have a built-in fuel reaction to generate the driving force. Considering that there was no chemical reaction on the convex surface of the microshell, no electroosmotic flow and ion gradient would be produced between the motor and the environment solution; thus, the motion mechanism of this FLM-C should be bubble propulsion[34] rather than diffusiophoresis[35] and electrophoresis.[36] Because the size of FLM-C was 2 μm, a small amount of O_2 would be produced; thus, only microbubbles but not big visible bubbles were generated. The bubble generation on the bowl structure of FLM-C was observed by a microscope (Figure 1G) through the opening upward immobilization of FLM-C (Figure S4). The periodic change in brightness in the microbowl (Figure 1H) presented the generation and burst of O_2 bubbles, and the duration of period represented the bubble growth time (Video S3).[37] Correspondingly, the intensity exhibited a periodic triangular pulse change in which the gradual increase and sharp reduction of the intensity were induced by the growth and burst of microbubbles, respectively. Surprisingly, after changing the surroundings of FLM-C from 100 mM H_2O_2 to 1 mM H_2O_2 and further to pure water, the periodic triangular pulse variation on the curve was retained, just its pulse frequency slowed down from $(99 \pm 21\ s)^{-1}$ to $(198 \pm 18\ s)^{-1}$ within 30 min. This result confirmed that the FLM-C could carry H_2O_2 fuel in its bowl shell to generate O_2 bubbles continuously in a fuel-free environment.

2.2. Motion of a 10 μm Hemispherical Shell Motor. We further studied the fuel-loading ability of a 10 μm hemispherical shell motor with a catalase engine (10-HSM-C) (Figure 2A). The 10-HSM-C showed fast translation motion at an average speed of 170.8 ± 10.9 μm/s in 500 mM H_2O_2 with propulsion from visible bubbles, which was generated at a high frequency and detached quickly from the microshell mouth. However, the motion of 10-HSM-C could only occur in a fuel environment; once they were exchanged into the pure water, their motion behavior disappeared immediately (Figure 2B,C and Video S4). Correspondingly, the bubble generation of 10-HSM-C was also observed only in a fuel environment (Figure 2D and Video S5). These results showed that 10-HSM-C did not have a fuel-loading ability.

2.3. Fuel-Loading Ability of Microshell Motors. The above experiments indicated that the hemispherical microshell only at a certain size could be used to prepare FLM. Actually, the concave bowl space of the hemispherical microshell acted

https://doi.org/10.1021/acsami.2c05442
ACS Appl. Mater. Interfaces 2022, 14, 27074−27082

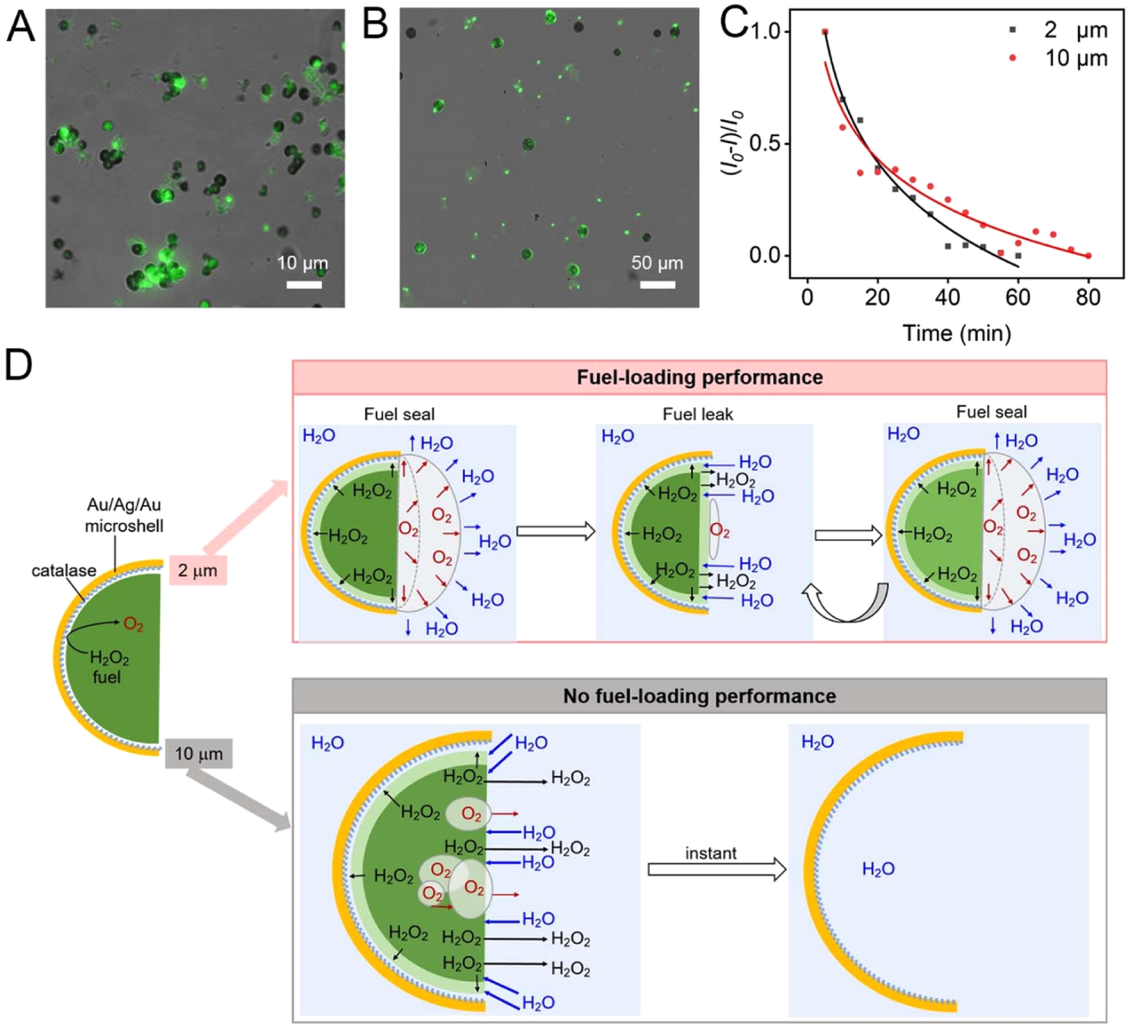

Figure 3. Fluorescence images of (A) 2 μm and (B) 10 μm hemispherical shells loading rhodamine B through capillary action. (C) Fluorescence intensity decrease percentage over time for microshell loading with rhodamine B in water. (D) Schematic description of bubble generation and H_2O_2 diffusion in water of FLM-C and 10-HSM-C.

as a natural container, and its fuel storage property was verified by fluorescent tracking rhodamine B. As expected, both 2 and 10 μm hemispherical shells were able to load rhodamine B solution based on capillary action (Figure 3A,B). Although the leakage of rhodamine B immediately occurred when these microshells were resoaked in water, the external diffusion of the loaded molecule from the concave bowl was a time-consuming process; for example, the complete leakage of rhodamine B in 2 and 10 μm shells required 40 and 55 min, respectively (Figure 3C and Video S6). Thus, we deemed the difference in the fuel-loading ability between 2 and 10 μm hemispherical shells to be due to the different bubble behaviors in their concave space. Figure 1H shows O_2 bubbles generated slowly and burst instantly in the 2 μm hemispherical shell motors. The generation of a bubble took about 100 s. Such a long-term growth of spherical-cap-shaped O_2 bubbles[38] on the fuel interface effectively prevented the contact of H_2O_2 and water, resulting in the fuel seal in the concave bowl space (Figure 3D). Fuel leak occurred only at the moment of bubble rupture and then returned to the fuel seal immediately. The periodic generation of bubbles resulted in sealing of the microshell mouth for most of the time, which endowed the 2 μm hemispherical shell motor with fuel-loading ability. On the contrary, O_2 bubbles generated rapidly for 10-HSM-C (Figure 2B). The highly frequent bubble generation not only went against the growth of the O_2 cap on the shell mouth but also aggravated the convection of H_2O_2 and water. Hence, the fuel in 10-HSM-C would be spilled out instantly to the surrounding water, resulting in the inability of fuel-loading for 10-HSM-C (Figure 3D).

2.4. Motion of FLM with a Pt Engine. The fuel-loading micromotor was not limited to a catalase engine but also to a Pt engine. Here, based on the 2 μm hemispherical Pt/Ag/Au shell, an FLM with a Pt engine (FLM-Pt) was constructed (Figure S5). FLM-Pt showed similar MSD curves as FLM-C in the fuel solution, indicating that the motion mechanism of FLM-Pt was also bubble propulsion (Figure 4A,B). FLM-Pt allowed the enhanced diffusion motion to last for 40 min in a fuel-free environment after one refueling (Figures 4C,D, and S6 and Video S7). The different endurance times between FLM-Pt and FLM-C should be due to the different catalytic capacities of catalase and Pt. Additionally, the motion of FLM-Pt with regular H_2O_2 recharging every 10 min was observed (Figure S7 and Video S8). The MSD curves along with the D value of FLM-Pt were stable throughout 70 min (Figure 4E,F),

https://doi.org/10.1021/acsami.2c05442
ACS Appl. Mater. Interfaces 2022, 14, 27074−27082

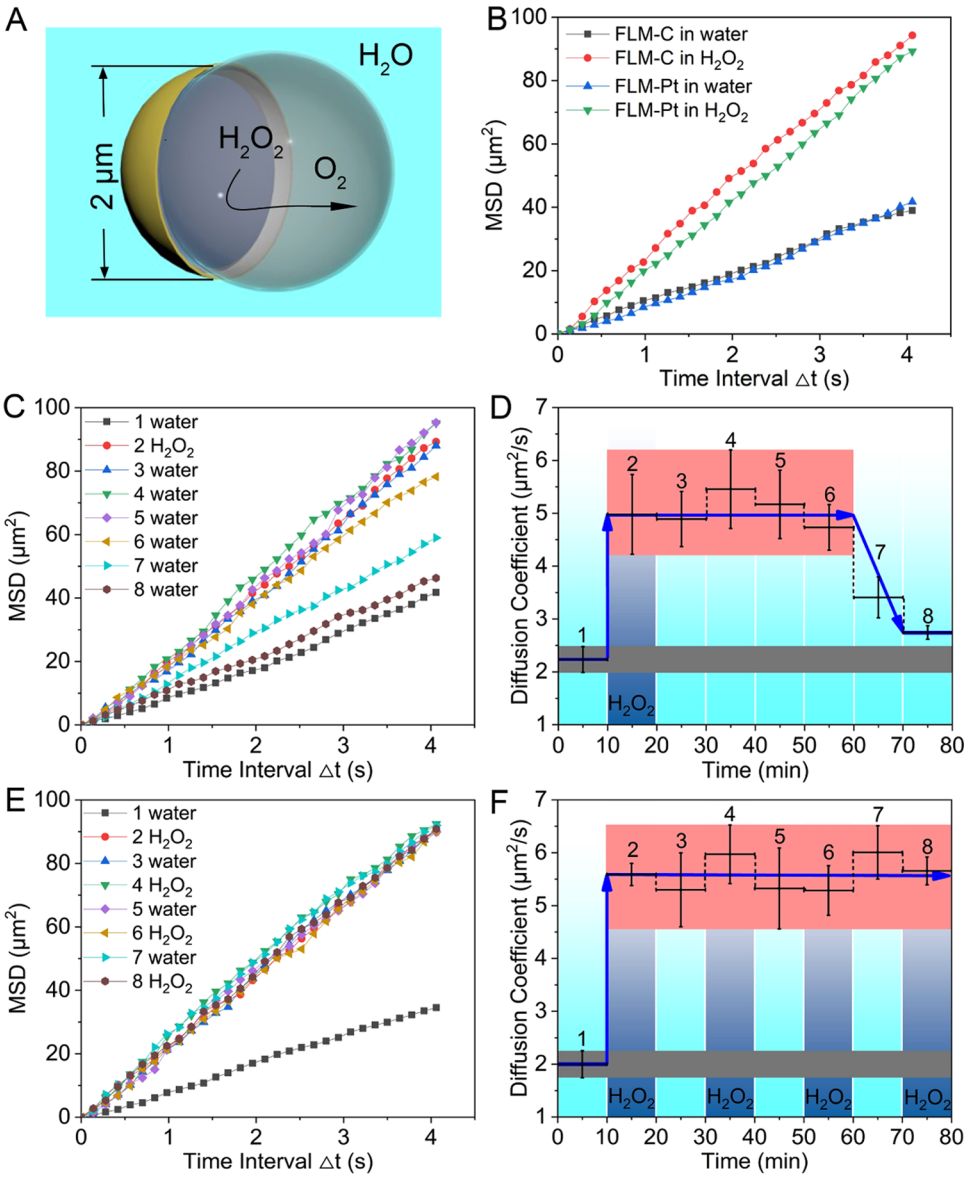

Figure 4. (A) Schematic generation of an O_2 bubble on FLM-Pt. (B) MSD plots of FLM-Pt and FLM-C. (C, E) MSD plots and (D, F) the corresponding diffusion coefficients of FLM-Pt successively in (C, D) and alternately in (E, F) water and 500 mM H_2O_2.

indicating that FLM-Pt also had the repeated fuel-loading performance.

2.5. Motion of a 10 μm Big-Enclosed Shell Motor. On the other hand, a 10 μm big-enclosed shell motor with a Pt engine (10-BSM-Pt) was fabricated to further investigate the fuel-loading ability of microshell motors (Figure 5A). The 10-BSM-Pt was prepared by magnetron sputtering, and the diameter of its open mouth was ~5 μm, in which the enclosed surface rate was ~90% (Figure S8). Compared to 10-HSM-C, 10-BSM-Pt was driven by bubbles generated at a lower frequency and exhibited a straight motion with a lower speed of 31.2 ± 2.7 μm/s (Figure 5B,C, and Video S9). However, bubble generation on 10-BSM-Pt continued when it was exchanged from H_2O_2 to a pure water environment (Figure 5D and Video S10). More interestingly, the growth of a single O_2 bubble on a microshell mouth from spherical-cap-shaped to big-ball-shaped was observed on 10-BSM-Pt in 5 M H_2O_2, and some O_2 bubbles could grow continuously for more than 70 min in water (Video S11). These results confirmed that H_2O_2 fuel could be sealed in the concave bowl of the microshell by an O_2 bubble covering the shell mouth. Additionally, although the lower bubble generation frequency was better for fuel sealing, it produced a smaller driving force, which was not conducive to motor movement; thus, no motion behavior was observed for 10-BSM-Pt in a fuel-free environment (Figure 5B,C, and Video S9).

2.6. Overall Discussion of the Fuel-Loading Microshell Motor. In this work, four kinds of microshell motors including 2-FLM-C, 10-HSM-C, 2-FLM-Pt, and 10-BSM-Pt were fabricated, and their motion performances were summarized in Table S1. The motion behavior of the microshell motors was determined by the size of shells, which was closely related to the size and generation efficiency of bubbles; for example, 2 μm shell motors (2-FLM-C and 2-FLM-Pt) exhibited enhanced diffusion due to the weak driving force from the microbubbles with a slow generation frequency, while 10 μm shell motors (10-HSM-C and 10-BSM-Pt) exhibited translation motion due to the strong driving force

https://doi.org/10.1021/acsami.2c05442
ACS Appl. Mater. Interfaces 2022, 14, 27074−27082

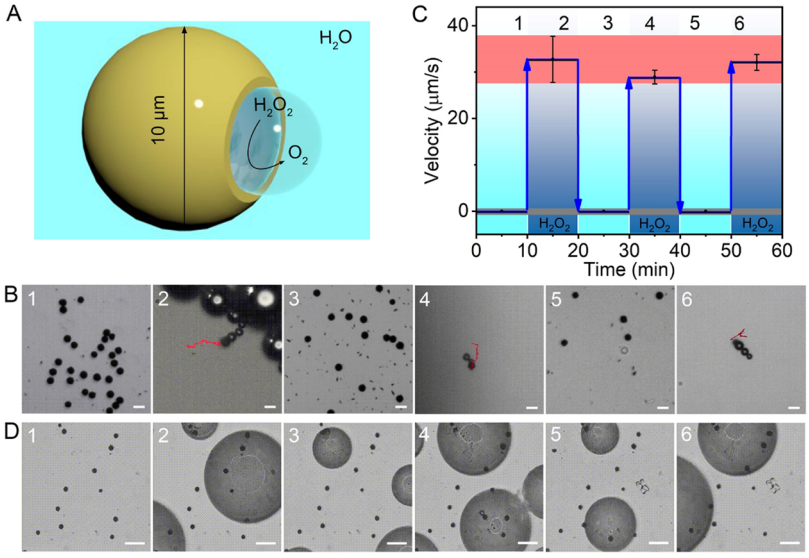

Figure 5. (A) Schematic generation of an O_2 bubble on 10-BSM-Pt. (B) Motion trajectories, (C) mean velocities, and (D) O_2 bubble generation of 10-BSM-Pt alternately in water (1, 3, 5) and 10 M H_2O_2 (2, 4, 6). Scale bars were 10 (B) and 50 μm (D).

from the big visible bubbles with a high generation frequency. Here, the fuel-loading motion ability was only observed on 2 μm shell motors (2-FLM-C and 2-FLM-Pt); however, the fuel seal ability was observed not only on 2-FLM-C and 2-FLM-Pt but also on 10-BSM-Pt. This result indicated that the fuel seal in the concave bowl space could be achieved on 10 μm microshells by reducing the bubble generation frequency; meanwhile, it also showed the possibility of constructing fuel-loading motors with translation motion based on 10 μm microshells via precise optimization of the open diameter, at which the O_2 generation frequency was favorable for both the driving force and the fuel seal.

The proposed micromotors (2-FLM-C and 2-FLM-Pt) achieved the continuous motion in a fuel-free environment based on their fuel-loading ability; hence, compared with other fuel-free micromotors such as enzyme-/Mg-/Zn-/Al-based micromotors, which required a specific biological fluid or acidic conditions,[22,39,40] this fuel-loading micromotor could completely mitigate the need of a motion environment and move in pure water. In addition, different from Mg-/Zn-/Al-based micromotors with a short lifetime, the proposed fuel-loading micromotors showed a 30 min continuous motion by one fueling and even permanent motion by repeated refilling. However, the application of the proposed fuel-loading micromotors is limited at present due to their slow enhanced diffusion motion.

3. CONCLUSIONS

In summary, a refillable fuel-loading micromotor was rationally fabricated to achieve persistent motion in a fuel-free environment. The micromotor was constructed on a 2 μm hemispherical multimetallic shell, like a vehicle, using a catalase (or Pt)-modified concave surface as the engine and the bowl shell structure as the fuel tank. H_2O_2 fuel could be drawn with capillary action into the microbowl and be decomposed by catalase (or Pt) to generate O_2 bubble capping on the microshell mouth, which resulted in a driving force as well as the fuel seal of the micromotor. The fuel-loading ability of microshell motors depended on the generation frequency of the O_2 cap, which was closely related to the size and morphology of microshells. The motion of the proposed fuel-loading micromotor could last for more than 30 min by one fueling, and permanent motion could be achieved with repeated refilling. Because the fuel-loading micromotor did not require the H_2O_2 fuel surrounding, it could be applied to systems against H_2O_2, for example, biological systems. Overall, the introduction of this refillable fuel-loading micromotor could address the problem of the real-time requirement of a fuel/energy surrounding by most synthetic motors, which provided the possibility of developing energy built-in micromotors for diverse applications.

4. EXPERIMENTAL SECTION

4.1. Materials and Reagents. All of the metals for deposition were supplied by Beijing Zhongjingkeyi Technology Co., Ltd. (China). Silicon dioxide microspheres (SiO_2 MPs) with different diameters were purchased from Shanghai Aladdin Bio-Chem Technology Co., Ltd. (China). Catalase from bovine, 11-mercaptoundecanoic acid (MUA), 6-mercapto-1-hexanol (MCH), *N*-hydroxycinimide (NHS), and 1-ethyl-3-(3-dimethylaminopropyl) carbodiimide hydrochloride (EDC) were purchased from Sigma-Aldrich. Hydrogen peroxide was supplied by Nanjing WANQING Chemical Grass ware & Instrument Co., Ltd. (China). Sodium cholate hydrate (NaCh) was bought from Alfa Aesar Chemical Co., Ltd. (China). Hydrofluoric acid (HF, 40%) and rhodamine B were purchased from Shanghai Macklin Biochemical Co., Ltd. (China). Other reagents used in this work were all of analytic grade. Ultrapure water was produced from a Millipore water purification system (≥18 MΩ, Milli-Q, Millipore).

4.2. Preparation of Micromotors. The multimetallic microshells were prepared via template-directed deposition. Before deposition, SiO_2 MPs dispersed in ethanol were dropped onto a glass substrate pretreated with Piranhas acid to form a monolayer as the template. After drying in air, Au (or Pt), Ag, and Au were sputtered successively to obtain a multimetallic coat on SiO_2 MPs. Here, E-beam and magnetron sputtering were chosen for the preparation of hemispherical microshells (Figures S1 and S5A) and big-enclosed microshells (Figure S8A), respectively. The thickness of these metal layers was size-dependent, and in this work, we chose 10:40:10 and 30:120:30 nm patterns for the fabrication of 2 and 10 μm shells, respectively. After ultrasonic treatment and washing, the metal-coated SiO_2 MPs were redispersed in PBS buffer (10 mM, pH 5.5).

https://doi.org/10.1021/acsami.2c05442
ACS Appl. Mater. Interfaces 2022, 14, 27074−27082

The above-prepared Au/Ag/Au-coated 2 μm SiO_2 MPs were used for the fabrication of FLM-C (Figure S1). First, these Janus microspheres were incubated with 1 mM MCH overnight to block the convex Au surface and then treated in 10% HF to etch SiO_2 templates and produce microshells. Afterward, the microshells were immersed in a mixture solution of 25 mM MUA and 1 mM MCH to form the MUA monolayer on their concave Au surface. Next, catalase was modified on the microshell concave via the reaction of its amino groups with hydroxyl groups of MUA, which were activated by 0.4 M EDC and 0.1 M NHS.

On the other hand, microshell motors with a Pt engine including FLM-Pt and 10-BSM-Pt were obtained just by dropping the Pt/Ag/Au-coated SiO_2 MPs into 10% HF (Figures S5A and S8A).

All of the above-mentioned micromotors were stored in PBS buffer at 4 °C before use.

4.3. Characterization of the Motion Behavior of Micromotors. Micromotors dispersed in the fuel (or fuel-free) solution were dropped on a clean glass slide. Then, their motion behaviors were observed and recorded by an inverted optical microscope (Leica DMI 3000B) equipped with a Photometrics Evolve 512/SC camera (Roper Scientific, Duluth, GA) at a frame rate of 10 frames/s. Trajectory tracking of micromotors was accomplished by Leica MM AF 1.5 software. Here, the fuel solution was a mixture of a certain concentration of H_2O_2 and 0.8% NaCh, and the fuel-free solution was pure water. The exchange of micromotors in fuel and fuel-free solutions was achieved by separating the motors from the present solution via two quick centrifugations and redispersed into the next solution.

4.4. Characterization of the Bubble Generation on FLM-C. For a clear observation, FLM-C was immobilized on glass slides with their opening upward (Figure S4). Here, the metal-coated SiO_2 MPs were incubated with a mixture of 25 mM MUA and 1 mM MCH before template etching, resulting in multimetallic microshells with the MUA layer on their convex surface. After activation with 0.4 M EDC and 0.1 M NHS, multimetallic microshells were dropped on the amino-functionalized glass slides for immobilization.

Au/Ag/Au microshells immobilized on the slide were then incubated with 1% ethanolamine to block excess activated carboxyl groups of convex MUA. Subsequently, they were covered with a mixture of 25 mM MUA and 1 mM MCH to form the MUA monolayer on their concave Au surface for further linking with the catalase, which resulted in the opening upward immobilization of FLM-C on the glass slide.

Fuel (a mixture of 100 mM H_2O_2 and 0.8% NaCh) and fuel-free (pure water) solutions were covered alternately on the slide to observe the bubble generation of FLM-C. During the solution exchange, the previous solution was rinsed away with water before the second solution was dropped. Images were captured and recorded by an inverted microscope at the frame rate of 1 fps. Bubble behaviors were further analyzed and quantified by Image J software.

4.5. Characterization of the Capillarity and External Diffusion of Microshells. Rhodamine B was used as a fluorescent molecular tracer for exploring the capillarity and external diffusion of microshells. First, the microshells immobilized on the glass slides were covered with 20 μM rhodamine B. After a quick yet full rinse with water, the microshells were re-covered with water and observed by an inverted fluorescent microscope. The images of microshells with rhodamine B were captured and recorded at different times, and the fluorescent intensity was further analyzed and quantified by Image J software.

■ ASSOCIATED CONTENT

Supporting Information

The Supporting Information is available free of charge at https://pubs.acs.org/doi/10.1021/acsami.2c05442.

Fabrication, characterization, and trajectories of FLM-C, FLM-Pt, and 10-BSM-Pt (Figures S1−S8) (PDF)

Motion of FLM-C successively in environments 1−8 (from a fuel-free environment to a fuel environment and then back to a fuel-free environment) with a 10 min presence in each environment (Video S1) (MP4)

Motion of FLM-C alternately in pure water (1, 3, 5) and a 500 mM H_2O_2 fuel solution (2, 4, 6) with a 10 min presence in each (Video S2) (MP4)

Bubble generation of FLM-C successively in environments from water to 100 mM H_2O_2, to 1 mM H_2O_2, and then to water, and finally to another water, with a 10 min presence in each environment (Video S3) (MP4)

Motion of 10-HSM-C alternately in pure water (1, 3, 5) and a 500 mM H_2O_2 fuel solution (2, 4, 6) with a 10 min presence in each environment (Video S4) (MP4)

Bubble generation of 10-HSM-C alternately in pure water (1, 3, 5) and a 100 mM H_2O_2 fuel solution (2, 4, 6) with a 10 min presence in each environment (Video S5) (MP4)

Capillarity adsorption and external diffusion of rhodamine B in 2 and 10 μm hemispherical microshells, respectively (Video S6) (MP4)

Motion of FLM-Pt successively from a fuel-free environment (1) to a fuel environment (2) and then back to fuel-free environments (3−8), with a 10 min presence in each environment (Video S7) (MP4)

Motion of FLM-Pt alternately in pure water (1, 3, 5, 7) and a 500 mM H_2O_2 fuel solution (2, 4, 6, 8) with a 10 min presence in each environment (Video S8) (MP4)

Motion of 10-BSM-Pt alternately in pure water (1, 3, 5) and a 10 M H_2O_2 fuel solution (2, 4, 6) with a 10 min presence in each environment (Video S9) (MP4)

Bubble generation of 10-BSM-Pt alternately in pure water (1, 3, 5) and a 10 M H_2O_2 fuel solution (2, 4, 6) with a 10 min presence in each environment (Video S10) (MP4)

Bubble generation of 10-BSM-Pt successively from a fuel environment (1) to serial fuel-free environments (2−8) with a 10 min presence in each environment (Video S11) (MP4)

■ AUTHOR INFORMATION

Corresponding Authors

Huangxian Ju − *State Key Laboratory of Analytical Chemistry for Life Science, School of Chemistry and Chemical Engineering, Nanjing University, Nanjing 210023, P. R. China;* orcid.org/0000-0002-6741-5302; Email: hxju@nju.edu.cn

Jie Wu − *State Key Laboratory of Analytical Chemistry for Life Science, School of Chemistry and Chemical Engineering, Nanjing University, Nanjing 210023, P. R. China;* orcid.org/0000-0003-1379-122X; Email: wujie@nju.edu.cn

Authors

Dong Wang − *State Key Laboratory of Analytical Chemistry for Life Science, School of Chemistry and Chemical Engineering, Nanjing University, Nanjing 210023, P. R. China*

Chengtao Chen − *State Key Laboratory of Analytical Chemistry for Life Science, School of Chemistry and Chemical Engineering, Nanjing University, Nanjing 210023, P. R. China*

Jun Sun − *State Key Laboratory of Analytical Chemistry for Life Science, School of Chemistry and Chemical Engineering, Nanjing University, Nanjing 210023, P. R. China*

https://doi.org/10.1021/acsami.2c05442
ACS Appl. Mater. Interfaces 2022, 14, 27074−27082

Hang Ao − *State Key Laboratory of Analytical Chemistry for Life Science, School of Chemistry and Chemical Engineering, Nanjing University, Nanjing 210023, P. R. China*

Wencheng Xiao − *State Key Laboratory of Analytical Chemistry for Life Science, School of Chemistry and Chemical Engineering, Nanjing University, Nanjing 210023, P. R. China*

Complete contact information is available at: https://pubs.acs.org/10.1021/acsami.2c05442

Author Contributions

‡W.D. and C.C. contributed equally.

Notes

The authors declare no competing financial interest.

■ ACKNOWLEDGMENTS

The authors gratefully acknowledge the National Natural Science Foundation of China (21575063, 21827812) and the Independent Research Foundation from State Key Laboratory of Analytical Chemistry for Life Science (5431ZZXM2006).

■ REFERENCES

(1) Zheng, S. H.; Wang, Y.; Pan, S. H.; Ma, E. H.; Jin, S.; Jiao, M.; Wang, W. J.; Li, J. J.; Xu, K.; Wang, H. Biocompatible Nanomotors as Active Diagnostic Imaging Agents for Enhanced Magnetic Resonance Imaging of Tumor Tissues In Vivo. *Adv. Funct. Mater.* **2021**, *31*, No. 2100936.

(2) Hortelão, A. C.; Patiño, T. A.; Perez-Jiménez, A.; Blanco, À.; Sánchez, S. Enzyme-Powered Nanobots Enhance Anticancer Drug Delivery. *Adv. Funct. Mater.* **2018**, *28*, No. 1705086.

(3) Lin, Z. H.; Gao, C. Y.; Wang, D. L.; He, Q. Bubble-Propelled Janus Gallium/Zinc Micromotors for the Active Treatment of Bacterial Infections. *Angew. Chem., Int. Ed.* **2021**, *60*, 8750−8754.

(4) Parmar, J.; Vilela, D.; Villa, K.; Wang, J.; Sánchez, S. J. Micro- and Nanomotors as Active Environmental Microcleaners and Sensors. *J. Am. Chem. Soc.* **2018**, *140*, 9317−9331.

(5) Gao, C. Y.; Wang, Y.; Ye, Z. H.; Lin, Z. H.; Ma, X.; He, Q. Biomedical Micro-/Nanomotors: From Overcoming Biological Barriers to In Vivo Imaging. *Adv. Mater.* **2021**, *33*, No. 2000512.

(6) Ma, X.; Jannasch, A.; Albrecht, U.; Hahn, K.; Miguel-López, A.; Schäffer, K.; Sánchez, S. Enzyme-Powered Hollow Mesoporous Janus Nanomotors. *Nano Lett.* **2015**, *15*, 7043−7050.

(7) Li, Z. S.; Zhang, H. Y.; Wu, Z. G.; He, Q. Acoustically-Propelled Rodlike Liquid Metal Colloidal Motors. *ChemNanoMat* **2021**, *7*, 1025−1029.

(8) Zhou, D. K.; Zhuang, R. C.; Chang, X. C.; Li, L. Q. Enhanced Light-Harvesting Efficiency and Adaptation: A Review on Visible-Light-Driven Micro/Nanomotors. *Research* **2020**, *2020*, 1−25.

(9) Salinas, G.; Tieriekhov, K.; Garrigue, P.; Sojic, N.; Bouffier, L.; Kuhn, A. J. Lorentz Force-Driven Autonomous Janus Swimmers. *J. Am. Chem. Soc.* **2021**, *143*, 12708−12714.

(10) Loget, G.; Kuhn, A. Electric Field-Induced Chemical Locomotion of Conducting Objects. *Nat. Commun.* **2011**, *2*, No. 535.

(11) Yuan, K. S.; Asunción-Nadal, V.; Jurado-Sánchez, B.; Escarpa, A. 2D Nanomaterials Wrapped Janus Micromotors with Built-in Multiengines for Bubble, Magnetic, and Light Driven Propulsion. *Chem. Mater.* **2020**, *32*, 1983−1992.

(12) Su, Y. J.; Ge, Y.; Liu, L. M.; Zhang, L. N.; Liu, M.; Sun, Y. Y.; Zhang, H.; Dong, B. Motion-Based pH Sensing Based on the Cartridge-Case-like Micromotor. *ACS Appl. Mater. Interfaces* **2016**, *8*, 4250−4257.

(13) Yi, D. L.; Zhang, Q.; Liu, Y. H.; Song, J. Y.; Tang, Y.; Caruso, F.; Wang, Y. J. Synthesis of Chemically Asymmetric Silica Nanobottles and Their Application for Cargo Loading and as Nanoreactors and Nanomotors. *Angew. Chem., Int. Ed.* **2016**, *55*, 14733−14737.

(14) Ji, Y. X.; Lin, X. K.; Zhang, H. Y.; Wu, Y. J.; Li, J. B.; He, Q. Thermoresponsive Polymer Brush Modulation on the Direction of Motion of Phoretically Driven Janus Micromotors. *Angew. Chem., Int. Ed.* **2019**, *58*, 4184−4188.

(15) Yuan, K. S.; Pacheco, M.; Jurado-Sánchez, B.; Escarpa, A. Design and Control of the Micromotor Swarm Toward Smart Applications. *Adv. Intell. Syst.* **2021**, *3*, No. 2100002.

(16) Xing, Y.; Zhou, M. X.; Du, X.; Li, X. Y.; Li, J. Q.; Xu, T. L.; Zhang, X. J. Hollow mesoporous carbon@Pt Janus nanomotors with dual response of H_2O_2 and near-infrared light for active cargo delivery. *Appl. Mater. Today* **2019**, *17*, 85−91.

(17) Laocharoensuk, R.; Burdick, J.; Wang, J. Carbon-Nanotube-Induced Acceleration of Catalytic Nanomotors. *ACS Nano* **2008**, *2*, 1069−1075.

(18) Ma, X.; Wang, X.; Hahn, K.; Sánchez, S. Motion Control of Urea-Powered Biocompatible Hollow Microcapsules. *ACS Nano* **2016**, *10*, 3597−3605.

(19) Li, Z. S.; Zhang, H. Y.; Wang, D. L.; Gao, C. Y.; Sun, M. M.; Wu, Z. G.; He, Q. Reconfigurable Assembly of Active Liquid Metal Colloidal Cluster. *Angew. Chem., Int. Ed.* **2020**, *59*, 19884−19888.

(20) Vyskočil, J.; Mayorga-Martinez, C. C.; Jablonská, E.; Novotný, F.; Ruml, T.; Pumer, M. Cancer Cells Microsurgery via Asymmetric Bent Surface Au/Ag/Ni Microrobotic Scalpels Through a Transversal Rotating Magnetic Field. *ACS Nano* **2020**, *14*, 8247−8256.

(21) Sridhar, V.; Park, B.; Sitti, M. Light-Driven Janus Hollow Mesoporous TiO_2−Au Microswimmers. *Adv. Funct. Mater.* **2018**, *28*, No. 1704902.

(22) Dey, K. K.; Zhao, X.; Tansi, B. M.; Méndez-Ortiz, W. J.; Córdova-Figueroa, U. M.; Golestanian, R.; Sen, A. Micromotors Powered by Enzyme Catalysis. *Nano Lett.* **2015**, *15*, 8311−8315.

(23) Lu, Z. J.; Gao, J. Y.; Fang, C.; Zhou, Y.; Li, X.; Han, G. R. Porous Pt Nanospheres Incorporated with GOx to Enable Synergistic Oxygen-Inductive Starvation/Electrodynamic Tumor Therapy. *Adv. Sci.* **2020**, *7*, No. 2001223.

(24) Hortelão, A. C.; García-Jimeno, S.; Cano-Sarabia, M.; Patiño, T.; Maspoch, D.; Sanchez, S. LipoBots: Using Liposomal Vesicles as Protective Shell of Urease-Based Nanomotors. *Adv. Funct. Mater.* **2020**, *30*, No. 2002767.

(25) Patino, T.; Porchetta, A.; Jannasch, A.; Llado, A.; Stumpp, T.; Schäffer, K.; Ricci, F.; Sánchez, S. Self-Sensing Enzyme-Powered Micromotors Equipped with pH-Responsive DNA Nanoswitches. *Nano Lett.* **2019**, *19*, 3440−3447.

(26) Xiong, K.; Xu, L. L.; Lin, J. W.; Mou, F. Z.; Guan, J. G. Mg-Based Micromotors with Motion Responsive to Dual Stimuli. *Research* **2020**, *2020*, No. 6213981.

(27) Ge, H. B.; Chen, X.; Liu, X. J.; Lu, X. L.; Gu, Z. W. Metal-Based Transient Micromotors: From Principle to Environmental and Biomedical Applications. *Chem. Asian J.* **2019**, *14*, 2348−2356.

(28) Sun, Y. Y.; Li, M. T.; Duan, R. M.; Zhang, D. F.; Zhang, H.; Song, B.; Dong, B. Reconfigurable XOR and INHIBIT Logic Gates Based on Multifuel-Driven Mg/Al Janus Micromotor. *Adv. Mater. Technol.* **2018**, *3*, No. 1800208.

(29) Zhou, M. Y.; Xing, Y.; Li, X. Y.; Du, X.; Xu, T. L.; Zhang, X. J. Cancer Cell Membrane Camouflaged Semi-Yolk@Spiky-Shell Nanomotor for Enhanced Cell Adhesion and Synergistic Therapy. *Small* **2020**, *16*, No. 2003834.

(30) Ye, Y. C.; Tong, F.; Wang, S. H.; Jiang, X. M.; Gao, J. B.; Liu, L.; Liu, K.; Wang, F.; Wang, Z.; Ou, J. F.; Chen, B.; Wilson, D. A.; Tu, Y. F.; Peng, F. Apoptotic Tumor DNA Activated Nanomotor Chemotaxis. *Nano Lett.* **2021**, *21*, 8086−8094.

(31) Jurado-Sánchez, B.; Pacheco, M.; Maria-Hormigos, R.; Escarpa, A. Perspectives on Janus Micromotors: Materials and Applications. *Appl. Mater. Today* **2017**, *9*, 407−418.

(32) Jiang, J. Z.; Ren, L. Q.; Huang, Y. P.; Li, X. D.; Wu, S. H.; Sun, J. J. 3D Nanoporous Gold-Supported Pt Nanoparticles as Highly Accelerating Catalytic Au-Pt Micromotors. *Adv. Mater. Interfaces* **2018**, *5*, No. 1701689.

(33) Xing, Y.; Pan, Q.; Du, X.; Xu, T. L.; He, Y.; Zhang, X. J. Dendritic Janus Nanomotors with Precisely Modulated Coverages

and Their Effects on Propulsion. *ACS Appl. Mater. Interfaces* **2019**, *11*, 10426−10433.
(34) Zhang, X. Q.; Chen, C. T.; Wu, J.; Ju, H. X. Bubble-Propelled Jellyfish-like Micromotors for DNA Sensing. *ACS Appl. Mater. Interfaces* **2019**, *11*, 13581−13588.
(35) Wang, W.; Duan, W. T.; Ahmed, S.; Mallouk, T. E.; Sen, A. Small Power: Autonomous Nano- and Micromotors Propelled by Self-Generated Gradients. *Nano Today* **2013**, *8*, 531−554.
(36) Lyu, X. L.; Liu, X. X.; Zhou, C.; Duan, D. S.; Xu, P. Z.; Dai, X.; Chen, X. W.; Peng, Y. X.; Cui, D. H.; Tang, J. Y.; Ma, X.; Wang, W. J. Active, Yet Little Mobility: Asymmetric Decomposition of H_2O_2 Is Not Sufficient in Propelling Catalytic Micromotors. *J. Am. Chem. Soc.* **2021**, *143*, 12154−12164.
(37) Su, H.; Fang, Y. M.; Chen, F. Y.; Wang, W. Monitoring the Dynamic Photocatalytic Activity of Single CdS Nanoparticles by Lighting Up H_2 Nanobubbles with Fluorescent Dyes. *Chem. Sci.* **2018**, *9*, 1448−1453.
(38) Lohse, D.; Zhang, X. H. Surface Nanobubbles and Nanodroplets. *Rev. Mod. Phys.* **2015**, *87*, 981−1035.
(39) de Ávila, B.-F.; Angsantikul, P.; Li, J.; Angel Lopez-Ramirez, M.; Ramirez-Herrera, D. E.; Thamphiwatana, S.; Chen, C.; Delezuk, J.; Samakapiruk, R.; Ramez, V.; Obonyo, M.; Zhang, L.; Wang, J. Micromotor-Enabled Active Drug Delivery for In Vivo Treatment of Stomach Infection. *Nat. Commun.* **2017**, *8*, No. 272.
(40) Karshalev, E.; Zhang, Y.; Esteban-Fernandez de Avila, B.; Beltran-Gastelum, M.; Chen, Y.; Mundaca-Uribe, R.; Zhang, F.; Nguyen, B.; Tong, Y.; Fang, R. H.; Zhang, L.; Wang, J. Micromotors for Active Delivery of Minerals toward the Treatment of Iron Deficiency Anemia. *Nano Lett.* **2019**, *19*, 7816−7826.

https://doi.org/10.1021/acsami.2c05442
ACS Appl. Mater. Interfaces 2022, 14, 27074−27082